Future arctic ocean primary productivity from CMIP5 simulations: Uncertain outcome, but consistent mechanisms

Martin Vancoppenolle, Laurent Bopp, Gurvan Madec, John Dunne, Tatiana Ilyina, Paul R. Halloran, Nadja Steiner

GLOBAL BIOGEOCHEMICAL CYCLES, VOL. 27, 605–619, doi:10.1002/gbc.20055, 2013

Future Arctic Ocean primary productivity from CMIP5 simulations: Uncertain outcome, but consistent mechanisms

Martin Vancoppenolle,[1] Laurent Bopp,[2] Gurvan Madec,[1,3] John Dunne,[4] Tatiana Ilyina,[5] Paul R. Halloran,[6,7] and Nadja Steiner[8,9]

Received 14 January 2013; revised 29 May 2013; accepted 2 June 2013; published 1 July 2013.

[1] Net Arctic Ocean primary production (PP) is expected to increase over this century, due to less perennial sea ice and more available light, but could decrease depending on changes in nitrate (NO_3) supply. Here Coupled Model Intercomparison Project Phase 5 simulations performed with 11 Earth System Models are analyzed in terms of PP, surface NO_3, and sea ice coverage over 1900–2100. Whereas the mean model simulates reasonably well Arctic-integrated PP (511 TgC/yr, 1998–2005) and projects a mild 58 TgC/yr increase by 2080–2099 for the strongest climate change scenario, models do not agree on the sign of future PP change. However, similar mechanisms operate in all models. The perennial ice loss-driven increase in PP is in most models NO_3-limited. The Arctic surface NO_3 is decreasing over the 21st century (-2.3 ± 1 mmol/m^3), associated with shoaling mixed layer and with decreasing NO_3 in the nearby North Atlantic and Pacific waters. However, the intermodel spread in the degree of NO_3 limitation is initially high, resulting from >1000 year spin-up simulations. This initial NO_3 spread, combined with the trend, causes a large variation in the timing of oligotrophy onset—which directly controls the sign of future PP change. Virtually all models agree in the open ocean zones on more spatially integrated PP and less PP per unit area. The source of model uncertainty is located in the sea ice zone, where a subtle balance between light and nutrient limitations determines the PP change. Hence, it is argued that reducing uncertainty on present Arctic NO_3 in the sea ice zone would render Arctic PP projections much more consistent.

Citation: Vancoppenolle, M., L. Bopp, G. Madec, J. Dunne, T. Ilyina, P. R. Halloran, and N. Steiner (2013), Future Arctic Ocean primary productivity from CMIP5 simulations: Uncertain outcome, but consistent mechanisms, *Global Biogeochem. Cycles*, *27*, 605–619, doi:10.1002/gbc.20055.

1. Introduction

[2] Rapid Arctic sea ice retreat has occurred over the last 10 years [e.g., *Stroeve et al.*, 2012], culminating in 2012 with a September annual minimum nearly 50% below the 1979–2000 average [*University of Colorado at Boulder*, 2012]. This retreat is associated with younger and thinner ice [*Maslanik et al.*, 2007; *Kwok and Rothrock*, 2009] and an increasingly long melt season [*Stammerjohn et al.*, 2012]. Summer ice retreat has the potential to profoundly impact the production of organic carbon by marine phytoplankton. Indeed, a 20% increase in net primary production (PP) annually integrated over the whole Arctic Ocean (hereafter, integrated primary production, I^{PP}, TgC/yr) from 1998 to 2009 has been inferred using a combination of satellite ice concentration and ocean color products [*Arrigo and van Dijken*, 2011]. This increase has been shown to be associated with sea ice retreat, not with increasing primary production per unit area (hereafter, specific primary production, *sPP*, mgC/m^2/yr). Ocean color data also suggests earlier bloom onsets in the Arctic [*Kahru et al.*, 2011]. Those changes in primary production have a number of potential important consequences on marine food webs [see *Tremblay et al.*, 2012, and references therein], as well as on the carbon cycle [*Bates and Mathis*, 2009; *Cai et al.*, 2010]. Along those changes, other ongoing physical and geochemical changes in the Arctic Ocean have also been suggested: warming, upper layer freshening, altered stratification, increased acidification, and, in the subarctic Pacific, increased hypoxia [e.g., *Carmack and McLaughlin*, 2011].

Additional supporting information may be found in the online version of this article.

[1]LOCEAN-IPSL, CNRS, Paris, France.
[2]LSCE-IPSL, CNRS, Gif-sur-Yvette, France.
[3]NOC, Southampton, UK.
[4]GFDL, Princeton, New Jersey, USA.
[5]MPI, Hamburg, Germany.
[6]Met Office Hadley Centre, Exeter, UK.
[7]School of Geography, College of Life and Environmental Sciences, University of Exeter, Exeter, UK.
[8]Fisheries and Oceans, Sidney, British Columbia, Canada.
[9]CCCMA, Victoria, British Columbia, Canada.

Corresponding author: M. Vancoppenolle, Laboratoire d'Océanographie et du Climat, IPSL Boîte 100, 4 Place Jussieu, FR-75252 Paris CEDEX 05 France. (martin.vancoppenolle@locean-ipsl.upmc.fr)

0886-6236/13/10.1002/gbc.20055

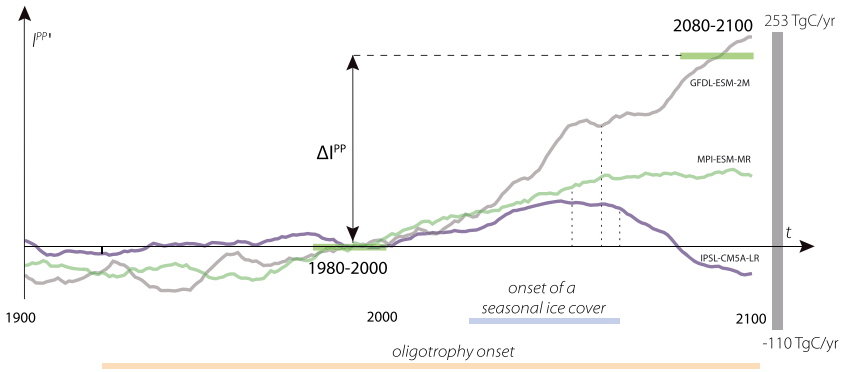

Figure 1. Typical evolution of Arctic Ocean I^{PP} anomalies (TgC/yr) over 1900–2100 (with respect to the 1980–2000 mean, 20 year running mean) from three selected CMIP5 models. The horizontal colored bars indicate: the 11-model range of the first year of oligotrophy (annual mean surface $NO_3 < k_{NO_3}$, orange); the first year with perennial ice extent < 10^6 km^2 (blue). The vertical gray bar on the right shows the range of I^{PP} change in 2080–2100 as compared to 1980–2000 (ΔI^{PP}). The vertical dotted lines indicate the first year with perennial ice extent < 10^6 km^2 for the three depicted models.

[3] Under increasing greenhouse forcing, sea ice retreat is projected to continue into the future [e.g., *Massonnet et al*., 2012]. Updated climate projections—performed in the framework of the World Climate Research Program Coupled Model Intercomparison Project Phase 5 (CMIP5) [*Taylor et al.*, 2012]—suggest a summer ice-free Arctic between 2041 and 2060 in a high-emission climate scenario [e.g., *Massonnet et al.*, 2012]. How primary production will evolve in the future Arctic Ocean depends on the present status and the future evolution of the limiting factors. Intuitively, sea ice retreat promotes phytoplankton growth via an increase of light availability. *Arrigo and van Dijken* [2011] project a >60% increase in I^{PP} for a summer ice-free Arctic using a simple linear extrapolation of the observed recent trends. This admittedly neglects potential nutrient limitation, as nitrate already limits primary production in some seasonally ice-covered Arctic locations [*Tremblay and Gagnon*, 2009]. However, the present and future role of nitrate limitation is difficult to assess. First, nutrient data are extremely scarce in the Arctic, and, second, the roles of factors directly controlling nitrate concentrations (ocean circulation, river runoff, atmospheric inputs, and biogeochemical recycling, including photo-oxidation) are not well understood [*Wassmann and Reigstad*, 2011].

[4] These uncertainties on phytoplankton growth limitation in the present Arctic are also obvious in ice-ocean model simulations of primary production forced by atmospheric reanalyses [*Popova et al.*, 2012]. These models show consistent spatial patterns of Arctic primary production and reasonable agreement with the satellite ocean color-based inferences of *Pabi et al.* [2008]. Moreover, whereas those models manifest similar levels of light limitation owing to the general agreement on the ice distribution, they disagree on the amount of nutrients available for primary production [*Popova et al.*, 2012]. Hence, the predictive capabilities of such models may be questionable as nutrient limitation could become increasingly important.

[5] Indeed, in an early model intercomparison using four Earth-System Models (ESMs) focusing on the response of marine primary production to climate change [*Steinacher et al*., 2010], the Arctic Ocean was identified as one of the regions where the models do not agree, with three ESMs showing increased primary production at the end of century, whereas one model shows decreased primary production. Here we find that 11 ESMs used for the new CMIP5 projections still disagree on the sign of future primary production change, primarily due to uncertainties in NO_3 concentrations (see Figure 1). Model simulations are analyzed using simulated vertically integrated net primary production, ice concentration, and surface nitrate concentration. In section 2, methods are described, including models, simulations, variables, and diagnostics of interest, as well as observational data sets used to evaluate models. In section 3, we first evaluate the ESMs simulations using historical data sets (section 3.1); then, we analyze projections for the late 21st century. Projections are analyzed for the whole Arctic region (section 3.2) and then separately for the open ocean and sea ice zones (section 3.3). We finally briefly discuss the stratification changes and their potential impact on NO_3. Results are discussed and conclusions are drawn in section 4.

2. Methodology

2.1. Description of Models and Simulations

[6] Table 1 lists and briefly describes the 11 ESMs used for this study. ESMs were selected on the requirement that they archived sea ice, primary production, and nitrate fields up to 2100 by the time of preparing this paper. We used the historical simulations from 1900 to 2005, and one climate change scenario, the *representative concentration pathway* (RCP) 8.5, for which the radiative forcing increases nearly steadily over the 21st century to peak at +8.5 W/m^2 in 2100 relative to preindustrial [*Moss et al.*, 2010]. Among the several ensemble members that were ran for each model, only the first one was analyzed.

[7] ESMs include representations of the general circulation and physics of the atmosphere, ocean, and sea ice, as well as several so-called *Earth System* processes, including biogeochemistry and carbon cycle for land and ocean. Among the models, different decisions were made with respect to the complexity of these components. Atmospheric

Table 1. A Brief Description of the ESMs Used in This Study

Model[a]	Atmosphere[b]	Ocean[c]	Sea Ice[c]	Marine Biogeochemistry[d]	Spinup (Offline+Online, Years)
CanESM2	35 lev., 2.8/2.8°	40 lev., 1.4/0.9°	CF, SM0L, 2lev	NPZD, 1 PG, N	6000 + 600
GFDL-ESM2G	24 lev., 2.0/2.5°	59 lev., 0.3°–1°	EVP, W00, ITD	30tr., 3 PG, N, P, Si, Fe	1 + 1000
GFDL-ESM2M	24 lev., 2.0/2.5°	50 lev., 0.3°–1°	EVP, W00, ITD	30tr., 3 PG, N, P, Si, Fe	1 + 1000
HadGEM2-CC	60 lev., 1.2/1.9°	40 lev., 0.3°–1°	EVP, SM0L, ITD	NPZD, 2 PG, N, Si, Fe	CMIP3 + x*1000+ 500 + 100
HadGEM2-ES	38 lev., 1.2/1.9°	40 lev., 0.3°–1°	EVP, SM0L, ITD	NPZD, 2 PG, N, Si, Fe	CMIP3 + x*1000 + 500 + 100
IPSL-CM5A-LR	39 lev., 1.9/3.8°	31 lev., 0.5°–2°	VP, SM3L, 2lev	24tr., 2 PG, NO3, NH4, P, Si, Fe	3000 + 300
IPSL-CM5A-MR	39 lev., 1.2/2.5°	31 lev., 0.5°–2°	VP, SM3L, 2lev	24tr., 2 PG, NO3, NH4, P, Si, Fe	3000 + 300
MIROC-ESM	80 lev., 2.8°	44 lev., 1.4/0.5°–1.7°	EVP, SM0L, 2lev	NPZD, 1 PG, N	1245 + 480
MIROC-ESM-CHEM[e]	80 lev., 2.8°	44 lev., 1.4/0.5°–1.7°	EVP, SM0L, 2lev	NPZD, 1 PG, N	1245 + 480
MPI-ESM-LR	47 lev., 1.9°	40 lev., 1.5°	VP, SM0L, 2lev	NPZD, 1 PG, N, P, Si, Fe	x*1000 + 1900
MPI-ESM-MR	95 lev., 1.9°	40 lev., 0.4°	VP, SM0L, 2lev	NPZD, 1 PG, N, P, Si, Fe	x*1000 + 1500

[a]References: Canadian Earth System Model (CanESM2) [*Arora et al.*, 2011; *Christian et al.*, 2010], Geophysical Fluid Dynamic Laboratory (GFDL) models [*Dunne et al.*, 2012, 2013], Hadley Centre Global Environmental (HadGEM) models [*HadGEM2 Team*, 2011; *Collins et al.*, 2011], Institut Pierre-Simon Laplace (IPSL) models [*Dufresne et al.*, 2013; *Aumont et al.*, 2003], Model for Interdisciplinary Research On Climate (MIROCs) [*Watanabe et al.*, 2011; *Kawamiya et al.*, 2000]; Max-Planck-Institut (MPI) models [*Ilyina et al.*, 2013; M. A. Giorgetta et al., Climate change from 1850 to 2100 in MPI-ESM simulations for the Coupled Model Intercomparison Project 5, submitted to *Journal of Advances in Modeling Earth Systems*, 2013].

[b]Number of vertical levels, longitude/latitude resolution of model grid.

[c]Sea ice model: dynamics, thermodynamics, and ice thickness distribution. CF = cavitating-fluid, EVP = Elastic-Viscous-Plastic, VP = Viscous-Plastic; W00 = *Winton* [2000] three-layer model, SM0L = *Semtner* [1976] zero-layer model, SM3L = *Semtner* [1976] three-layer model; ITD = multicategory representation of the subgrid-scale ice thickness distribution included; 2lev = two-level ice-open water formulation.

[d]Structure of the pelagic ecosystem model (NPZD = fixed quota Nutrient-Phytoplankton-Zooplankton-Detrital Matter Model, if more elaborated than NPZD, the number of transported tracers is indicated); number of phytoplankton groups (PG), limiting nutrients.

[e]Compared to MIROC-ESM, MIROC-ESM-CHEM includes an atmospheric chemical component.

(oceanic) horizontal grid resolution ranges over 1°–4° (0.5°–2°) and the number of vertical levels ranges from 24 to 95 (31 to 59).

[8] All models have reasonable sea ice dynamics. Regarding sea ice thermodynamics, most models still use the *Semtner* [1976] zero-layer model which is known to misrepresent the phase of the sea ice seasonal cycle. Four models include a representation of the subgrid-scale ice thickness distribution, which significantly improves the seasonality of both ice extent and thickness [*Massonnet et al.*, 2011] and sea-ice related feedbacks [*Holland et al.*, 2006]. Typically, there is no effective transmission of light through the ice itself, only the open water in the pack contributes: solar radiation which penetrates through the ocean surface linearly increases with simulated open water fraction.The only exceptions are the Geophysical Fluid Dynamics Laboratory (GFDL) models, which also enable light penetration through ice, depending on surface albedo, snow depth, and ice thickness.

[9] As far as the representation of marine biogeochemistry and microbial marine ecosystems is concerned, models can be divided in three groups. CanESM2 and the two MIROCs are the most simple in that respect, using an NPZD component with a single phytoplankton group and one limiting nutrient (N). The MPI-ESMs and HadGEM2s use enhanced NPZD models, including more limiting nutrients and an additional phytoplankton group for the HadGEM2s. At the end of the range, the IPSL and GFDL models use >20 tracers, including several phytoplankton and zooplankton groups, as well as an exhaustive ensemble of limiting nutrients, with, for some of them, varying quotas in the different model groups. Besides these differences in ecosystem model structure, there are also differences on how the model treat riverine and atmospheric inputs, sediment remobilization, and nitrogen fixation.

[10] In order to eliminate any spurious model drift, the initialization of the models starts from climatologies or from CMIP3 output. It then typically includes several thousand years of the offline ocean, sea ice, and marine biogeochemical component and then, a few hundred years of the fully coupled model (see Table 1). Therefore, the initial fields reflect the model equilibrium state rather than the observed values.

2.2. Diagnostics Used for Analysis

[11] The Arctic Region is our domain of interest. It encompasses all the oceanic pixels located north of the Arctic Circle (66.56°N) as in *Arrigo and van Dijken* [2011]. We use model output for ice concentration, nitrate concentration, and PP, as described below. All fields were interpolated on a 1° geographic latitude-longitude grid for the analysis.

[12] To characterize *sea ice*, we use monthly fields of *ice concentration* $A(\lambda, \phi, t)$ (*sic* in the CMIP5 terminology), which is the fractional surface of a grid cell covered by sea ice. λ and ϕ are latitude and longitude. Ice concentration is used to split the Arctic Region into time- and model-dependent zones: (i) the *ice zone* (IZ), i.e., the ensemble of cells with at least 15% of ice at least 1 month a year, (ii) the *perennial ice zone* (PIZ), i.e., the cells with at least 15% of ice in September, month of the annual minimum, (iii) the *seasonal ice zone* (SIZ), i.e., the cells that are in the IZ but not in the PIZ, and (iv) the *open ocean zone* (OZ), i.e., the cells that are not in the IZ. Note that 15% is a commonly used threshold to remove cells with small ice concentration values from the IZ. The extent of each zone is simply the integrated surface of area of its grid cells.

[13] Since nitrogen is the limiting nutrient in the Arctic Ocean, we characterize *nutrients* based on the annual mean fields of surface nitrate concentration $NO_3(\lambda, \phi, t)$ ($mmol/m^3$) (*no3* in the CMIP5 terminology). Ideally, the annual maximum nitrate value would have been a better measure of the potential for primary production, but was not available for all models. However, the annual maximum time series could be computed for nine models and

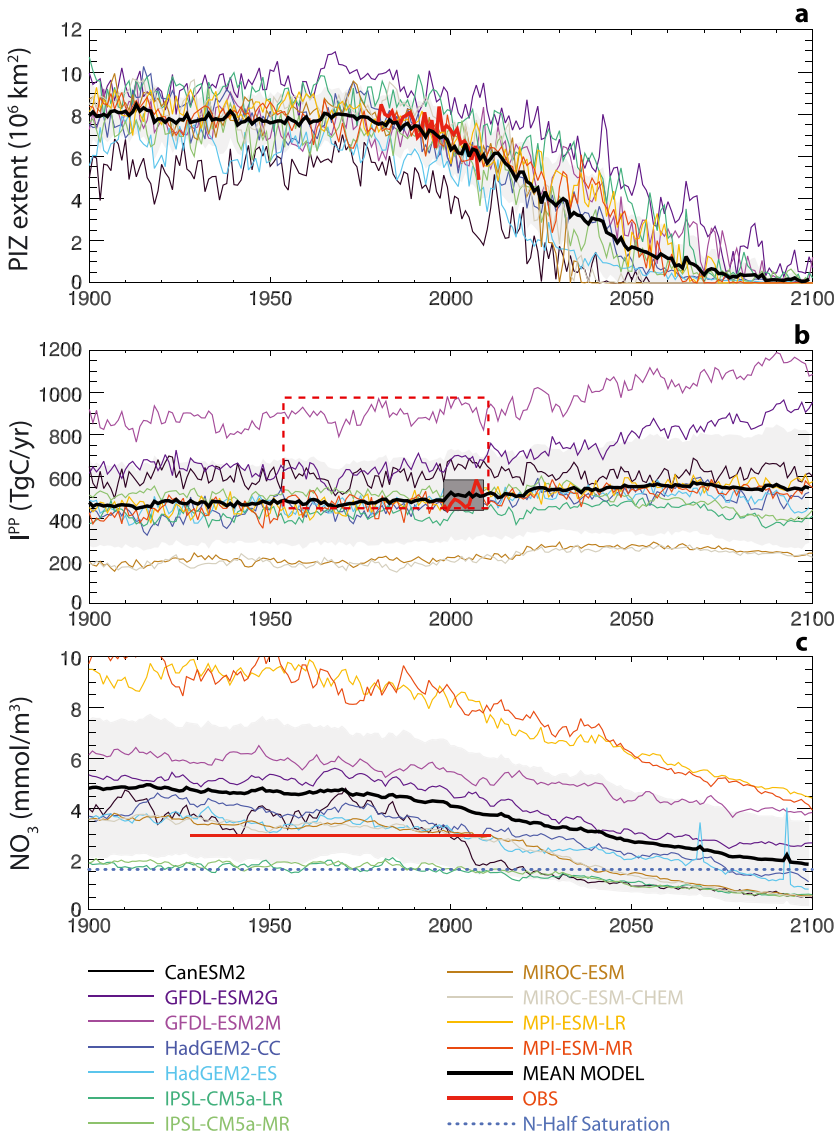

Figure 2. 1900–2100 yearly time series of (a) perennial ice zone (PIZ) extent, (b) integrated PP (I^{PP}), and (c) mean surface NO_3 over the whole Arctic, shown for the individual models (colored thin lines) and the mean model (thick black line), with the one standard deviation range (grey surface). Thick red lines are observations: (a) European Organisation for the Exploitation of Meteorological Satellites (EUMETSAT)-Ocean and Sea Ice Satellite Application Facility (OSISAF) passive microwave sea ice extent [*Tonboe et al.*, 2011], (b) satellite ocean-color PP [*Arrigo and van Dijken*, 2011] (solid) and in situ estimates [*Hill et al.*, 2013] (dash), and (c) World Ocean Atlas (WOA) NO_3 [*Garcia et al.*, 2010], which is not representative of the entire domain, due to low data coverage in the Arctic Basin. The half-saturation concentration for diatom NO_3 uptake [*Sarthou et al.*, 2005] uptake on Figure 2c indicates the oligotrophic threshold.

was found to be highly correlated (0.99) with the annual mean, over 1900–2100. Therefore, annual mean nitrate can be used as a valid replacement for trend analysis in the present context. In contrast, mean nitrate is not as good as a predictor for actual summer NO_3 limitation, but analysis in section 3.2 shows it is reasonably efficient for interpretation of the integrated primary production time series.

[14] We characterize *primary production* based on the annual fields of vertically integrated net primary mole productivity of carbon by all types of phytoplankton (*intpp* in the CMIP5 terminology), and convert it into *specific primary production* $sPP(\lambda, \phi, t)$ (gC/m^2/yr). Integrating spatially, we obtain the *integrated primary production* $I^{PP}(t)$ (TgC/yr). Dividing by the area of a given region, we obtain the *specific regional primary production* $\overline{sPP}$ (gC/m^2/yr) for that particular region.

[15] Analysis of time series is facilitated if *normalized* values are used. Normalized integrated primary production for a given year and a given model is defined as $I^{PP^*}(y) = I^{PP}(y)/I^{PP}(1900)$. Normalized average nitrate concentration is defined as $NO_3^*(y) = (NO_3(y) - 1.5 \times k^{NO_3})/NO_3(1900)$, where $k^{NO_3} = 1.6$ mmol/m^3 is the half-saturation concentration for

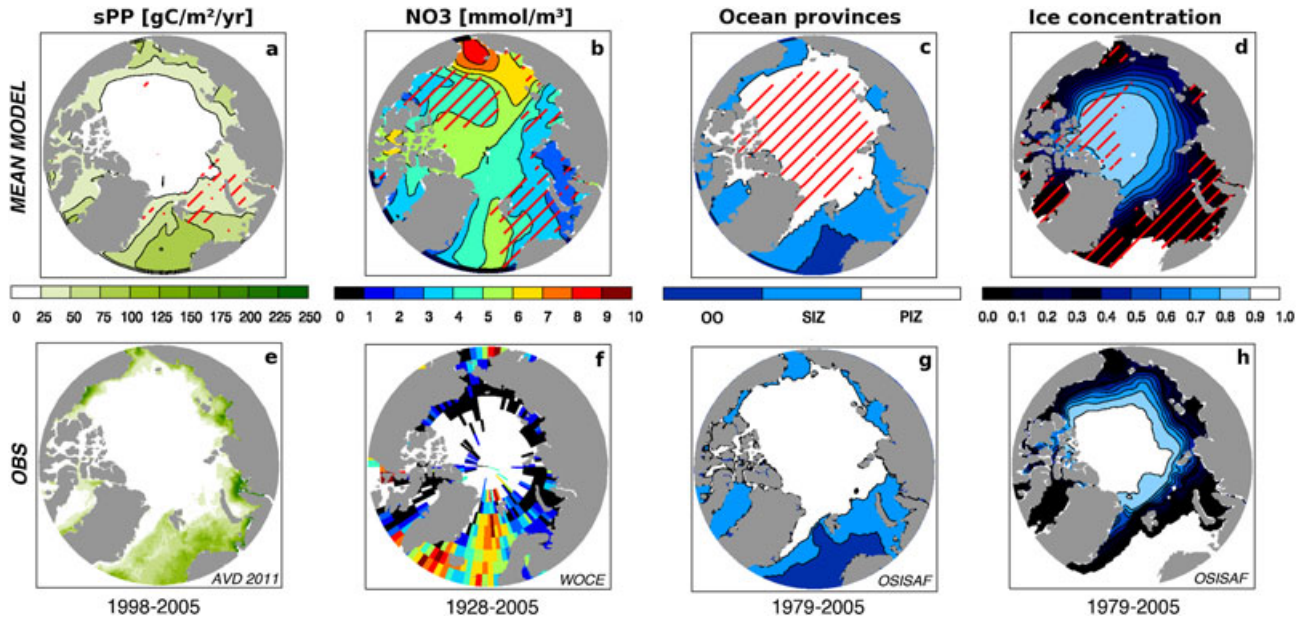

Figure 3. Evaluation of the historical simulation using observational data sets. (top) Mean model spatial distributions of (a) annual mean *sPP* (gC/m^2/yr), (b) surface annual mean NO_3 (mmol/m^3), (c) ocean provinces (OZ = open ocean zone, SIZ = seasonal ice zone, PIZ = perennial ice zone, see text for definitions), and (d) September ice concentration. Hatched zones indicate model spread: for Figures 3a, 3b, and 3d, they show where 80% of the models depart from model mean by less than one standard deviation; for Figure 3c, they show where 80% of the models have perennial ice. (bottom) Corresponding observations, namely, (e) satellite ocean-color *sPP* [*Arrigo and van Dijken*, 2011], (f) World Ocean Atlas (WOA) surface NO_3 [*Garcia et al.*, 2010], and (g, h) passive microwave EUMETSAT-OSISAF sea ice retrievals [*Tonboe et al.*, 2011]. Similar results for the individual models can be found in the supporting information (Figure S1).

nitrate uptake by diatoms [*Sarthou et al.*, 2005]. The multiplication by 1.5 is performed because nitrate limitation as formulated in the models starts for $NO_3 \sim 1.5 \times k^{NO_3}$. Using this formulation, NO_3^* is > 0 for supposed eutrophic conditions and < 0 for oligotrophic conditions.

[16] We had no access to the actual values of the *factors limiting diatom production* in the models, but we could to some extent reconstruct them, since the different limitation functions are generally expressed quite similarly among the models. For nitrate, we used the standard hyperbolic dependence:

$$lim_{NO_3}(y) = \frac{NO_3(y)}{k^{NO_3} + NO_3(y)}. \quad (1)$$

For limitation by light, we first noticed that, assuming no light transmission through sea ice (true for most models), the annual average incoming photosynthetically available radiation (PAR) is well correlated with September ice extent, or equivalently, the perennial ice zone extent S_{PIZ} (correlation = 0.89). Hence, for light, we use a limitation function based on the PIZ extent and the total surface area of the domain S_{dom}:

$$lim_{sie} = \frac{S_{dom} - S_{PIZ}(y)}{S_{dom}}. \quad (2)$$

The combined light-nutrient limitation function is defined as: $lim = lim_{NO_3} \cdot lim_{sie}$. We refer to the resulting expressions as *empirical* limitation functions, to emphasize that those are not the actual limitation functions, but rather an indirect measure of diatom growth limitation in the models. Empirical limitation functions have a value ~ 1 for weak limitation of diatom growth and ~ 0 for strong limitation.

2.3. Data Used for Validation

[17] Several observational products are used to evaluate the models historical simulations. *Primary production* data were calculated using the latest reprocessing (R2010.0) of surface Chl-a derived from 8 day Level 3 binned SeaWiFS ocean color measurements [*Pabi et al.*, 2008; *Arrigo and van Dijken*, 2011]. This derivation is based on the following. Chl-a is assumed to be constant over a prescribed (20 m) mixed-layer and to decrease exponentially further down into the water column. Using formulations for temperature response and light limitation of phytoplankton growth, daily net primary production (mgC/m^2/d) is derived for each satellite pixel. Using sea ice data and spatiotemporal extrapolation procedures, integrated primary production (TgC/yr) is derived for each year. The temporal (March–September) and spatial coverage are limited, as detailed in *Pabi et al.* [2008]. Here the 1998–2011 time series of integrated primary production (TgC/yr) (see Figure 2b) and the spatial distribution of annual specific primary production on a 9 km grid (1998–2005) (see Figure 3e) are used. Let us caution that satellite primary production retrievals underestimate vertically integrated production. This is because they are based on surface chlorophyll estimates and do not resolve the frequent subsurface chlorophyll maxima [*Tremblay et al.*, 2008]. A

brand new synthesis of primary production data in the Arctic Ocean [*Hill et al.*, 2013] suggests that Arctic-integrated PP increases from 466 ± 94 TgC/yr to 993 ± 94 TgC/yr when subsurface maxima are included.

[18] We use surface *nitrate* data from the World Ocean Atlas (WOA) [*Garcia et al.*, 2010] (see Figure 2c). The 2544 valid data points could be extracted above the Arctic circle, covering 1928–2005. Data coverage is sparse, with practically no data in the Arctic basin and an important summer bias [*Popova et al.*, 2012].

[19] *Sea ice concentration* data (1979–2007) derive from scanning multichannel microwave radiometer (SMMR) and the Special Sensor Microwave/Imager (SSM/I), reprocessed by the EUMETSAT Ocean and Sea Ice Satellite Application Facility [*Tonboe et al.*, 2011].

3. Results

3.1. Model Evaluation

[20] To evaluate the models, we analyze the results of the historical simulations and compare them to observational products. We find that primary production—both in terms of domain integral and spatial distribution—is rather realistic in the mean model, but highly variable among individual models. This is due to (i) a correct localization of the PIZ for the mean model and (ii) large intermodel differences in the factors controlling PP (sea ice and, in particular, NO_3).

[21] **Domain-integrated values**. The first three columns of Table 2 display the values of I^{PP}, NO_3, and the surface of the perennial ice zone (S_{PIZ}) over the last decade of the 20th century. Figure 2 shows the time series of integrated production, mean surface nitrate, and PIZ extent for all models over 1900–2100 and how they compare to observational estimates.

[22] Mean model I^{PP} is reasonably realistic, reaching 511 ± 12 TgC/yr over 1998–2005, compared with the 469 ± 16 TgC/yr derived from satellite ocean color data. The range from in situ observations [*Hill et al.*, 2013] is much larger (466–993 TgC/yr). However, the intermodel spread is large, reaching 40% of the mean, MIROC-ESM-CHEM (206 TgC/yr) and GFDL-ESM2M (947 TgC/yr) being the least and most productive models over 1998–2005, respectively.

[23] Mean model surface NO_3 is 4.5 ± 2.5 mmol/m^3 over 1928–2005, compared with an observed 3.0 mmol/m^3. This comparison has to be interpreted carefully, as the uncertainty on observed NO_3 is high above the Arctic circle, with almost no WOA observations in the Arctic Basin [see Figure 3f and *Popova et al.*, 2012]. Besides, the intermodel spread in NO_3 is large, reaching 55% of the mean, IPSL-CM5A-LR (1.7 mmol/m^3) and MPI-ESM-LR (9.1 mmol/m^3) showing the least and most surface NO_3 concentrations, respectively.

[24] The extent of the perennial ice zone (PIZ) over 1979–2005 is relatively well represented in the mean model (7.1 ± 0.5 million km^2), compared with an observed 7.4 ± 0.6 million square kilometers. The intermodel spread in PIZ extent is less than for I^{PP} and NO_3, reaching only 17% of the mean. CanESM2 (4.6 million km^2) and GFDL-ESM2G (9.0 million km^2) are the two extreme models in terms of PIZ extent over 1979–2005.

Table 2. Simulations Statistics for Each Model and the Mean Model[a]

Model	I^{PP} (TgC/yr)	$\overline{NO_3}$ (mmol/m^3) 1980–1999	S_{PIZ} (10^6km^2) 1980–1999	$\overline{h_{mld}^{max}}$ (m)	I^{PP} (TgC/yr)	$\overline{NO_3}$ (mmol/m^3) 2080–2099	S_{PIZ} (10^6km^2) 2080–2099	$\overline{h_{mld}^{max}}$ (m)	ΔI^{PP} (TgC/yr) (2080–2099) – (1980–1999)	$\overline{dI^{PP}/dt}$ (TgC/yr^2) 2080–2099	T_{olig} (yr)	T_{SIZ} (yr)
CanESM2	607.2	3.5	4.9	96.9[b]	627.4	0.6	0.0	74.5[b]	20.2	–0.9±1.2	2017	2021
GFDL-ESM2G	644.4	5.0	9.2	96.2[b]	897.3	2.6	1.2	68.6[b]	252.9	5.3±1.2	n.a.	2076
GFDL-ESM2M	900.9	5.6	6.9	97.5[b]	1132.7	3.9	0.3	84.6[b]	231.8	2.9±1.4	n.a.	2057
HadGEM2-CC	453.5	3.6	7.1	55.8[c]	491.2	1.4	0.1	57.5[c]	37.7	1.0±1.2	2077	2051
HadGEM2-ES	486.5	3.3	5.8	62.8[c]	484.7	1.3	0.0	59.8[c]	–1.7	–3.7±1.2	2075	2035
IPSL-CM5A-LR	417.0	1.7	8.8	65.4[b]	391.1	0.6	0.4	55.4[b]	–25.8	–1.0±0.7	1921	2062
IPSL-CM5A-MR	517.8	1.8	6.9	91.3[b]	407.8	0.6	0.3	59.1[b]	–110.0	–0.7±0.4	1942	2047
MIROC-ESM	206.6	3.2	7.5	100.0[c]	239.3	0.7	0.0	76.6[c]	32.7	–1.1±0.2	2039	2030
MIROC-ESM-CHEM	180.8	3.2	8.3	108.7[c]	232.7	0.6	0.0	77.5[c]	51.9	–0.5±0.2	2043	2033
MPI-ESM-LR	480.7	8.6	7.4	168.5[b]	567.9	4.8	0.0	124.4[b]	87.3	0.9±0.9	n.a.	2049
MPI-ESM-MR	469.5	8.9	7.3	196.0[b]	536.5	4.6	0.0	120.9[b]	67.0	–0.9±0.9	n.a.	2054
MEAN MODEL	487.7	4.4	7.3	103.6	546.2	2.0	0.2	78.3	58.5	0.2±0.3	n.a.	2062

[a]Annual primary production (domain integral, I^{PP}); surface NO_3 concentration (domain average, $\overline{NO_3}$); surface area of the perennial ice zone (S_{PIZ}); and seasonal maximum mixed layer depth (domain average, $\overline{h_{mld}^{max}}$); over 1980–1999 and 2080–2099. We also give ΔI^{PP}, the 2080–2099 to 1980–1999 change in I^{PP} (domain integral); $a = \overline{dI^{PP}/dt}$, the linear regression coefficient from the fit $I^{PP}(y) = a \cdot y + b$ (over 2080–2099); T_{olig}, the year where oligotrophy is attained (e.g., $\overline{NO_3} < k^{NO_3}$) for the first time; and T_{SIZ}, the year where S_{PIZ} falls below 10^6 km^2 for the first time.
[b]Mixed layer depth directly diagnosed from the vertical mixing scheme (*omlmax*).
[c]*T* and *S*-derived mixed layer depth (*mlotst*) provided by individual modelling groups, as *omlmax* was not available from the CMIP5 archive.

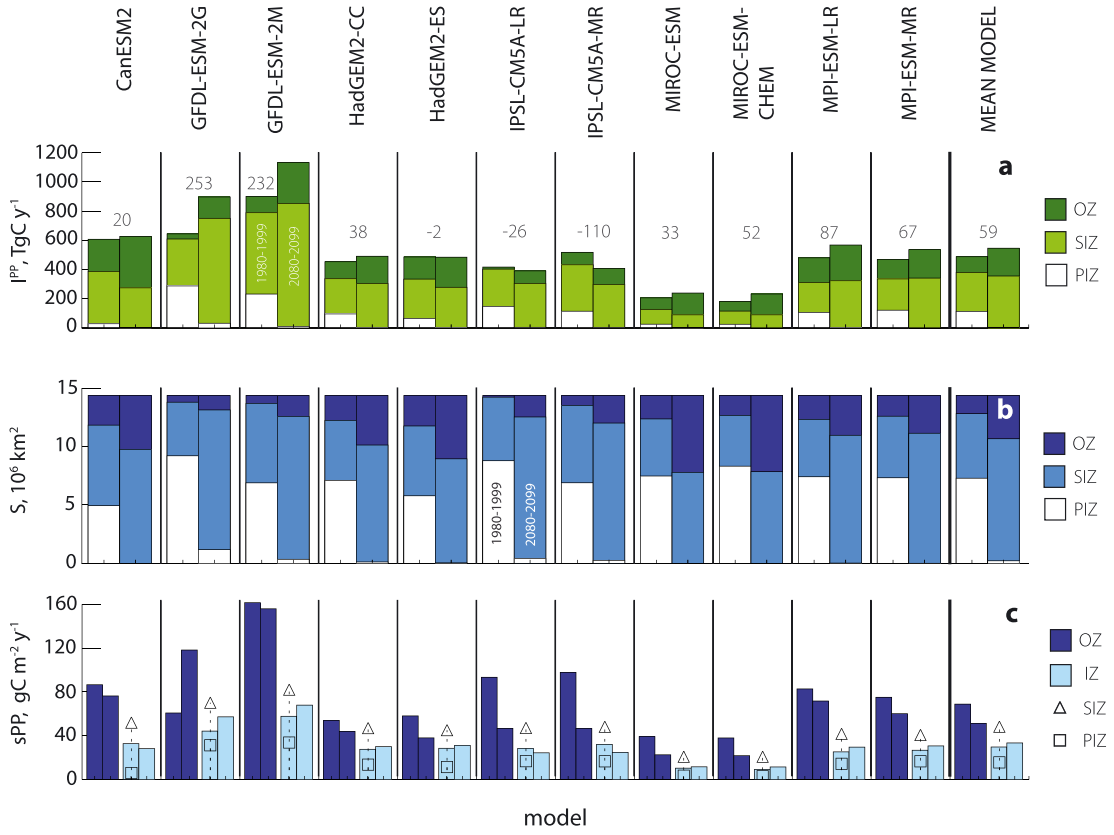

Figure 4. (a) I^{PP} (20 year averages) for each model over 1980–1999 (left members of each pair of bars) and 2080–2099 (right members), split into subregional contributions. The numbers (in TgC/y) give the 2080–2099 to 1980–1999 difference in domain-integrated I^{PP}. (b) Same, but for the surface area of those subregions. (c) *sPP* for the sea ice (white) and open ocean (blue) zones, for each model. Left (right) members of each pair of bars refer to 1980–1999 (2080–2099). Open symbols depict the 1980–1999 averages over the seasonal and perennial ice zones.

[25] The spread in I^{PP} is driven by the differences in the factors controlling primary production, namely nitrate concentration and sea ice. The associated corresponding empirical limitation factors are highly variable among models (see Figure S2). For 1980–1999, phytoplankton growth is typically more limited by sea ice than by nutrients, as indicated by the smaller empirical limitation factor for sea ice (0.49) than for nitrate (0.73) (mean model, 1980–1999). The intermodel range in both limitation factors is significant, from 0.36 (GFDL-ESM2G) to 0.66 (CanESM2) for sea ice; and from 0.51 (IPSL-CM5A-LR) to 0.85 (MPI-ESM-MR) for NO_3.

[26] **Spatial distributions**. The spatial distribution of specific primary production (see Figures 3a, 3e, and S1) is similar to satellite ocean-color retrievals, with near-zero values in the PIZ and maxima on the Siberian shelves, in the Chukchi Sea, and in the North Atlantic sectors of the Arctic Ocean. Large intermodel variations exist, however. For instance, the simulated maxima found near river mouths on the West Siberian shelves are highly variable and not as large as observed. In addition, both GFDL models have a significant share of under-ice production. Under-ice production cannot be detected from satellites but is supported by in situ observations [e.g., *Alexander and Niebauer*, 1981; *Mundy et al.*, 2009; *Arrigo et al.*, 2012]. The two HadGEM2s have high productivity on the East Siberian shelf and in the Chukchi Sea, and the two MIROCs simulate small specific primary production overall (see Figure S1).

[27] The spatial distribution of surface NO_3 is even more variable than that of *sPP* (see Figures 3b–3f and S1). The simulated NO_3 maximum in the North Atlantic is also found in WOA observations (see Figures 3b–3f), while the Chukchi Sea maximum is not, which could be due to a sampling summer bias in the WOA observations or to model parameterizations affecting Pacific water inflow. Indeed, one would expect an Atlantic-Pacific NO_3 gradient across the Arctic, as Pacific waters entering the Arctic tend to have higher NO_3 concentrations than Atlantic waters [*Codispoti et al.*, 2013]. Each model has specific regional characteristics. For instance, the mean model NO_3 maximum in the Chukchi Sea is only due to the contribution of four models (MPIs and HadGEM2s). CanESM2, IPSL, and MIROC models generally show weak NO_3 variations. The other models typically feature one large regional maximum, in the North Atlantic for the GFDL models, on the East Siberian Shelf for the HadGEM2 models, and a broad maximum centered in the Pacific Arctic for both MPI models (which have the largest NO_3 values in the sample).

[28] The 1979–2005 spatial distribution of the PIZ is well simulated in the mean model and by most models

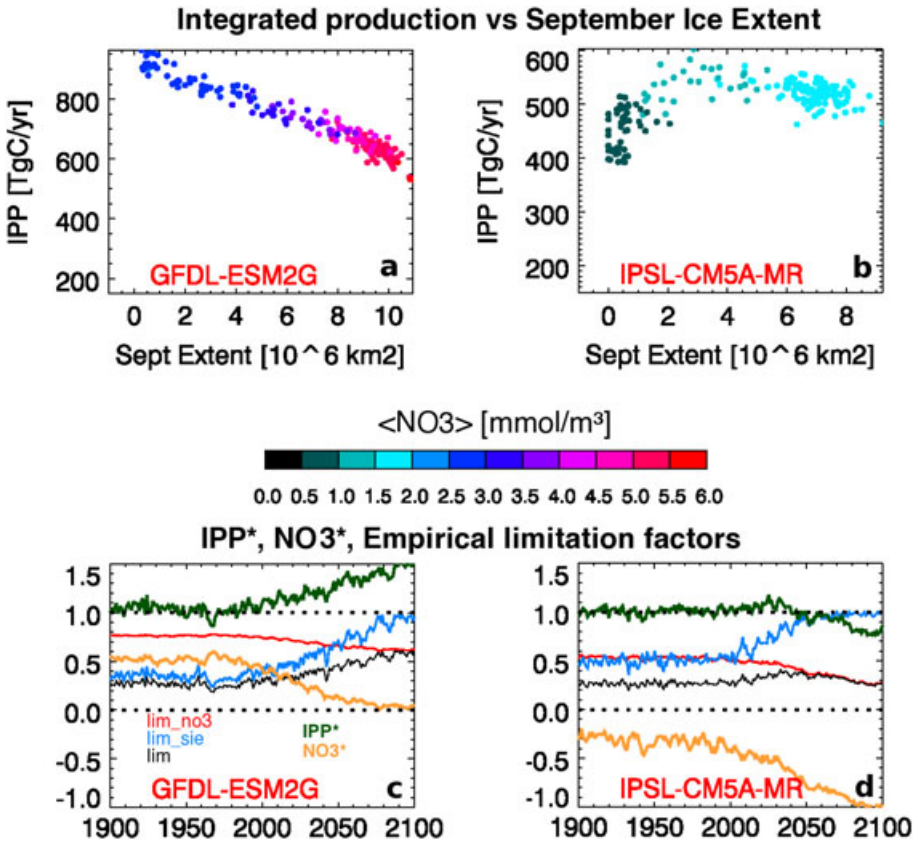

Figure 5. Analysis of 1900–2100 yearly time series for GFDL-ESM2G and IPSL-CM5A-MR models. (a, b) I^{PP} versus September ice extent. Colors refer to domain averages of NO_3 concentration (mmol/m^3). (c, d) Time series of I^{PP^*}, NO_3^* (normalized), and empirical limitation factors for nitrate (lim_{NO_3}), ice extent (lim_{sie}), and the product of both (lim). See section 2.2 for details on the computations. Similar results for all individual models can be found in the supporting information (Figure S2).

(see Figures 3c, 3d, 3g, 3h, and S1). The IZ extent is typically slightly overestimated, especially on the East of Greenland. The September concentration field is more variable among models, but intermodel differences are consistent with the location of the PIZ. Notable models are CanESM2 and HadGEM2-ES (summer low bias), as well as IPSL-CM5A-LR (winter high bias).

3.2. Response of Primary Production to Climate Change: The Arctic Ocean

[29] Summer ice extent and nitrogen levels both sharply decrease over the 21st century for all models (Figure 2 and Table 2). In contrast, the I^{PP} time series widely differ among models: for some models, I^{PP} increases continuously (e.g., GFDL's); for some, it remains rather stable (e.g., CanESM2); and for the rest of the models, I^{PP} initially increases, reaches a temporary maximum, then decreases (e.g., IPSL's). To quantify changes, we define ΔI^{PP} as the difference in 2080–2099 mean I^{PP} from the 1980 to 1999 mean (see Table 2 and Figure 4a). Over 11 models, two models predict a large increase (GFDLs); six predict a mild increase (e.g., $\Delta I^{PP} < 100$ TgC/yr, CanESM2, HadGEM2-CC, MIROCs, and MPIs); and three predict a decrease (IPSLs and HadGEM2-ES). In addition, among the six models with a mild positive ΔI^{PP}, I^{PP} is stable over 2080–2099 in two models and decreases in four models (see $\overline{dI^{PP}/dt}$ in Table 2). For those models, the cumulated decrease has not been sufficient yet to bring I^{PP} below the 1980–1999 levels. Note that because of different choices for ecosystem formulations and parameters, the GFDL models have an efficiently recycling microbial loop, inducing that a significant part of production is regenerated (much higher fraction than in the other models). This partly explains why I^{PP} increases in response to warming for those two models.

[30] These intermodel differences in the response of I^{PP} to climate change are due to the differences in the absolute values of the limiting factors, namely summer ice extent and NO_3. As their effect on primary production is opposite, the response of I^{PP} to climate change results from a subtle balance between an increase due to sea ice retreat and a decrease due to decreasing NO_3 stocks.

[31] To illustrate this, two models with extreme and opposite responses were selected (see Figure 5). GFDL-ESM2G has large initial NO_3 stocks and maintains NO_3 surface concentrations above the alleviated oligotrophic threshold throughout the 21st century ($NO_3^* > 0$, orange line, Figure 5c). Hence, integrated annual production (green) monotonically increases, following the empirical limitation factor (lim, black), which is primarily driven by the sea ice retreat (lim_{sie}, blue).

[32] In contrast, IPSL-CM5A-MR has much lower initial NO_3 levels, which are below the oligotrophic threshold

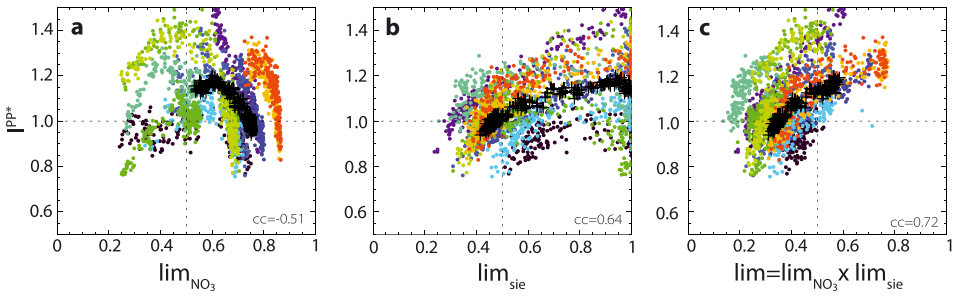

Figure 6. Yearly time series-based scatter plots (1900–2100) of normalized integrated production I^{PP*} versus (a) nitrate limitation factor, (b) ice extent limitation factor, and (c) combined nitrate-sea ice limitation factor. Symbols refer to the mean model (black plus signs) and the individual models (colored disks). See section 2.2 for details on the computations. Mean correlation coefficient is also given.

already at the beginning of the 20th century ($NO_3^* < 0$, orange line, Figure 5d). Hence, the release of light limitation due to sea ice retreat (blue) is counter-balanced by the increase in NO_3 limitation (red). In the early 21st century, the effect of sea ice retreat initially dominates, and the limitation factor (*lim*, black) and primary production (green) both increase. By about 2030, the effect of decreasing nutrients takes over, production decreases, and reaches levels below its 20th century values by about 2050.

[33] This analysis was performed for all models (see Figure S2), and for each of them, the change in I^{PP} is determined by the balance between the gains due to decreasing sea ice and the losses due to decreasing NO_3 stocks. This information is illustrated in a more synthetic fashion in Figure 6, where annual values of normalized integrated production I^{PP*} are plotted versus the limiting factors in several forms. Analysis indicates the following. (i) Above oligotrophy ($lim_{NO_3} > 0.5$, Figure 6a), I^{PP*} decreases with NO_3^*, just because sea ice decreases and nutrient increases are simultaneous. As expected, below oligotrophy, I^{PP*} is primarily controlled by and proportional to NO_3. (ii) In all models, production positively responds to decreasing summer ice extent (increasing lim_{sie}, Figure 6b). When the summer ice extent is too small, it cannot affect I^{PP*}, as shown by the large scatter of points at the right-end of Figure 6c. (iii) Only the combined effect of NO_3 and sea ice completely explains the changes in I^{PP*} (Figure 6c). Hence, we argue that changes in I^{PP} can be explained using the combination of nitrate and sea ice limitation factors.

[34] In this context, it seems that the uncertainty in NO_3 rather than the uncertainty in perennial ice extent explains the wide range in ΔI^{PP}. Indeed, oligotrophy is attained (see T_{olig} in Table 2) occurs as early as 1921 in IPSL-CM5A-LR, in the course of the 21st century for most models, or does not occur at all in the GFDL and MPI models. This range is much larger than the range in the first year where the perennial ice zone extent falls below 10^6 km^2 (2021 to 2076, see T_{SIZ} in Table 2).

[35] The mean model also shows an initial increase in primary production due to ice retreat, followed by a decrease driven by the NO_3 progressive depletion. This latter decrease is not sufficient to compensate for the initial sea ice effect, and the net change in I^{PP} is a +58 TgC/yr anomaly by the end of the 21st century (Table 2). Given the range of future I^{PP} projections in the Arctic, the mean model is not as meaningful as the full range of model responses, which well illustrates the role of initial NO_3 stocks on the uncertainty in I^{PP} projections.

3.3. Response of Primary Production to Climate Change: Spatial Variations

[36] The spatial distribution of the end-of-21st century changes in *sPP* (see Figure 7 and S3) indicates that surface NO_3 concentrations decrease in the whole domain and for all models, while *sPP* tends to consistently decrease in the OZ and to increase in the IZ, with large intermodel variations. As the OZ and IZ seem to be characterized by different responses, their contribution to I^{PP} was split for 1980–1999 and for 2080–2099 (Figure 4).

[37] By the end of the 20th century, the mean model IZ dominates (78%) I^{PP}. The IZ share is nevertheless smaller than the areal fraction of the IZ (89%), because *sPP* is more than twice as large (68.9 gC/m^2/yr) in the OZ than in the IZ (29.7 gC/m^2/yr). This *sPP* difference is attributable to specific physical characteristics of the two provinces (latitude, the presence of sea ice, and ocean vertical mixing). The share of the PIZ contribution to I^{PP} varies among models and is notably the largest in the GFDL models (25–44% of production in the PIZ), which allow light penetration through sea ice itself.

[38] By the end of the 21st century, the perennial ice zone typically disappears and the seasonal ice zone slightly decreases (Figure 8b); hence, the share of the IZ to I^{PP} decreases, while the specific primary production slightly increases to 33.4 gC/m^2/yr in the IZ (longer open water season) and decreases to 51.3 gC/m^2/yr in the OZ (less nutrients).

[39] To better understand how the OZ and IZ contribute to (2080–2099) to (1980–1999) changes in I^{PP}, their different contributors (TgC/yr) are depicted in Figure 8c for the mean model and detailed in Figure 4 and Table 3 for all models. The numbers in Table 3 are obtained as follows. We first split the domain change in I^{PP} into contributions from the sea ice and open ocean zones:

$$\Delta I^{PP} = \Delta I^{PP}_{IZ} + \Delta I^{PP}_{OZ}. \quad (3)$$

For any subregion of the domain, I^{PP} can be decomposed into $I^{PP} = S.\overline{sPP}$, where S is the surface of the subregion and $\overline{sPP}$ is the mean specific primary production over the subregion.

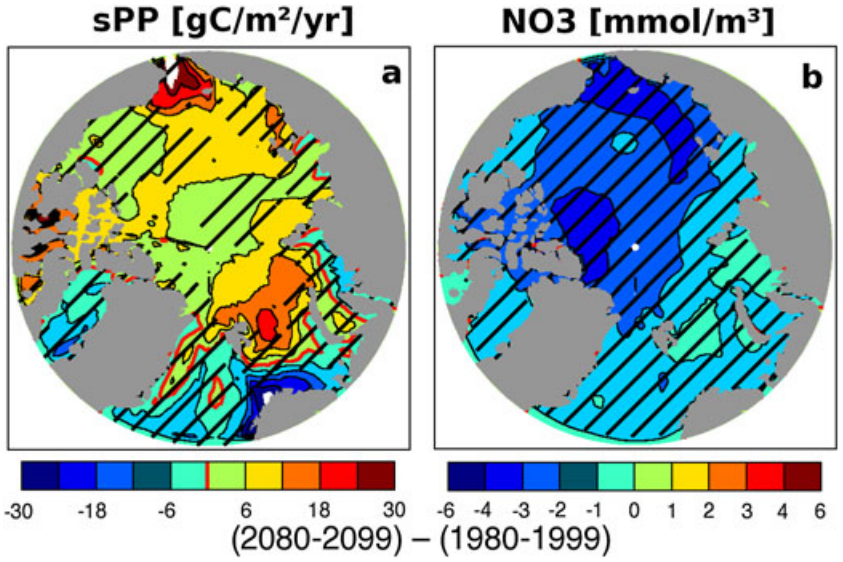

Figure 7. Spatial distribution of mean model 2080–2100 differences with respect to 1980–2000 for (a) annual *sPP* and (b) nitrate concentration. Hatched regions indicate where 80% of the models agree on the sign of the change. For *sPP*, similar results for all individual models can be found in the supporting information (Figure S3).

Hence, one can further separate ΔI^{PP} into contributions from changing S and $\overline{sPP}$:

$$\Delta I^{PP} = S.\Delta\overline{sPP} + \Delta S.\overline{sPP} \quad (4)$$

Using (4) to expand both terms on the right-hand side of equation (3) and using the fact that $\Delta S_{IZ} = -\Delta S_{OZ}$, we obtain a second decomposition for ΔI^{PP}:

$$\Delta I^{PP} = S.\Delta\overline{sPP}|_{IZ} + S.\Delta\overline{sPP}|_{OZ} + \Delta S_{IZ}.(\overline{sPP}_{IZ} - \overline{sPP}_{OCZ}), \quad (5)$$

where the first and second terms correspond to changing specific primary production in the sea ice and open zones, respectively, and the third term is the replacement of ice-covered regions into year-round open ocean.

[40] We first analyze the mean model 2080–2099 increase in I^{PP} with respect to 1980–1999, ΔI^{PP} = 58 TgC/yr. Based on (3), we find that ΔI^{PP} results from an OZ gain of 82 TgC/yr that is not fully canceled by an IZ loss of 24 TgC/yr. These 24 TgC/yr result from losses due to a reduced IZ extent (–68 TgC/yr), which dominate the gains due to increasing *sPP* in the IZ (43 TgC/yr). The 82 TgC/yr contribution of the OZ to ΔI^{PP} result from the gain due to the areal increase of the OZ (129 TgC/yr), dominating the losses due to the decrease in *sPP* in the OZ (–46 TgC/yr). This mean model behavior is characteristic of most models.

[41] Using equation (5), these 58 TgC/yr can be summarized as the sum of three processes: (i) an increase in *sPP* in the IZ (+43 Gt C/yr), likely because sea ice is more seasonal; (ii) a decrease in *sPP* in the low latitude OZ, typically the North Atlantic (-46 Gt C/year), because the ocean is more oligotrophic; and (iii) the conversion of >2 million km^2 of ice-covered regions into about twice as productive permanent open ocean (61 TgC/yr), which is the main contributor. The areas where sea ice disappear yearlong are typically the Greenland and Barents Seas (see Figure 8a).

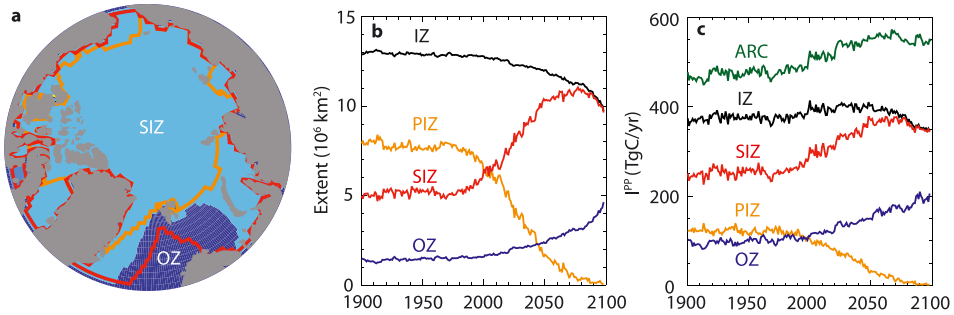

Figure 8. (a) Mean model location of the ocean provinces over 2080–2099 (colored surfaces, see section 2.2 for definitions), with the mean outer limits of the SIZ (red contour) and PIZ (orange) over 1980–1999. (b) Mean model time series of the extent of the different provinces. (c) Mean model time series of integrated primary production over the different provinces, completed by the domain total (ARC, green).

Table 3. (2080–2099) to (1980–1999) Changes in Integrated Primary Production (TgC/yr) Over the Arctic Region, for Each Model and the Mean Model[a]

Model	ΔI^{PP}	ΔI^{PP}_{IZ}	ΔI^{PP}_{OZ}	$S.\Delta\overline{sPP}\|_{IZ}$	$S.\Delta\overline{sPP}\|_{OZ}$	$\Delta S_{IZ}.(\overline{sPP}_{IZ}-\overline{sPP}_{OCZ})$	$\Delta S.\overline{sPP}\|_{IZ}$	$\Delta S.\overline{sPP}\|_{OZ}$
CanESM2	20.2	–112.3	132.5	–48.9	–36.8	105.9	–63.4	169.3
GFDL-ESM2G	252.9	141.7	111.2	175.1	52.3	25.5	–33.4	58.9
GFDL-ESM2M	231.8	63.7	168.1	133.0	–6.9	105.8	–69.3	175.1
HadGEM2-CC	37.7	–32.8	70.5	27.7	–32.1	42.2	–60.5	102.6
HadGEM2-ES	–1.7	–56.3	54.5	27.5	–80.5	51.2	–83.8	135.0
IPSL-CM5A-LR	–25.8	–98.2	72.4	–53.5	–46.3	74.0	–44.7	118.7
IPSL-CM5A-MR	–110.0	–135.2	25.2	–92.7	–82.7	65.4	–42.5	107.8
MIROC-ESM	32.7	–37.5	70.2	12.8	–71.4	91.4	–50.3	141.7
MIROC-ESM-CHEM	51.9	–25.9	77.8	23.8	–66.2	94.3	–49.7	144.0
MPI-ESM-LR	87.3	12.8	74.5	50.0	–30.3	67.6	–37.2	104.8
MPI-ESM-MR	67.0	5.3	61.7	47.3	–37.2	56.9	–42.0	98.9
Mean Model	58.5	–24.3	82.8	43.5	–46.2	61.2	–67.8	129.0

[a]This change (ΔI^{PP}) is decomposed into contributions from changes in area and specific primary production over the sea ice and open ocean zones. See section 3.3 for details.

[42] All models consistently feature an increase in open ocean I^{PP} due to the increase in open ocean area, and a simultaneous reduction in *sPP* in the OZ. In the IZ, the models disagree on the sign of the I^{PP} change and predict an increase for some (GFDLs, MPIs) and a decrease for others. Note that the GFDL models are peculiar, because they lose their perennial ice cover in the 21st century, recycle nitrogen more efficiently than the rest of the models, and have under-ice light transmission. In general, the models with increasing I^{PP} in the IZ are the ones for which increases in specific primary production dominates the losses due to the conversion from IZ to OZ. Those models are also the ones that are not oligotrophic (GFDL, MPI). This underlines again that information on nutrient levels in the IZ are crucial.

[43] We finally come back to the actual spatial distributions of *sPP* and NO_3 changes for 2080–2099 as compared to 1980–1999 (Figure 7). The Barents and Chukchi Seas see the most notable *sPP* increases. The Barents Sea moves from the IZ to the OZ in most models, while the Chukchi Sea typically remains in the IZ. More importantly, both regions are *inflow shelves* [*Carmack and Wassmann*, 2006], in the sense that they receive an external NO_3 supply (from Atlantic and Pacific waters, respectively) which can support the *sPP* increase. NO_3 decreases everywhere, particularly in the Arctic Basin and in the Chukchi Sea, and less so in other shelf regions, including Barents Sea. The factors explaining this contrast are: contrasting mixed layer trends in deep basins (decrease) and in the vicinity of the shelf break (increase); and long advective time scales between the Arctic Basin and Pacific, Atlantic (T = 15–20 years) and shelf (T = 5 years) waters sources [*Popova et al.*, 2013]. The NO_3 decrease is larger in the Chukchi Sea than in other shelf regions, because of the increasing NO_3 uptake associated with the *sPP* increase.

3.4. Factors Contributing to the NO_3 Uncertainties and Trend

[44] The large intermodel NO_3 scatter is present from the beginning of the simulations; therefore, it must be linked to various initialization strategies. NO_3 initial fields reflect the model equilibrium state, reached after long (>1000 year) spin-ups simulations.

[45] Despite the large intermodel scatter, surface NO_3 consistently decreases in all models at a mean rate of 2.3 ± 1 mmol/m^3/century over the 21st century. This can be due to increased stratification, decreased Pacific and Atlantic NO_3 concentrations, weaker Atlantic and Pacific water inflows, and increased N export to depth by sinking particles. Quantifying those processes through a N budget is not feasible with the available CMIP5 data. A quick look at the evolution of the seasonality of NO_3 indicates that winter NO_3 concentrations are smaller and smaller every year, indicating that nutrient stocks decrease. This can be explained by the decreasing NO_3 physical supply, being less and less able to compensate for the biological N uptake and export to depth. In the rest of this section, we show that throughout the 21st century, most models simulate (i) a stratification increase in the entire Arctic region and (ii) a surface NO_3 decrease in the North Atlantic and North Pacific that is quite comparable to the Arctic one.

[46] To quantify stratification, consistently defined mixed-layer depths (h_{mld}) for all models were not available. The best compromise was to use the monthly maximum mixed layer depth from vertical mixing scheme (*omlmax* in the CMIP5 terminology) for seven models and the mixed layer diagnosed from T and S vertical profiles (*mlotst*) for the HadGEMs and MIROCs (see Table 2). Since these two definitions are not consistent, the mean model is not really meaningful and was given for indication only.

[47] Over 1980–1999, simulated mixed layers show an ample seasonal cycle with a March maximum of $h^{max}_{mld} \sim$ 100 m (mean model, Arctic Region) and a summer minimum of ∼ 10 m. The simulated h^{max}_{mld} is much larger in the OZ (∼ 600 m) than in the IZ (∼ 100 m).

[48] By 2080–2099, h^{max}_{mld} is typically 25 m smaller than the 1980–1999 average for the whole model ensemble. In Figure 9, time series of the following stratification index

$$SI(t) = \frac{\tilde{h}^{max}_{mld}(t)}{\overline{h^{max}_{mld}}|_{1900-1910}} - 1 \quad (6)$$

are plotted for the entire Arctic, the sea ice, and open ocean zones. $\tilde{h}$ refers to a 5 year running mean and $\overline{h}$ refers to a regular mean. *SI* cancels the differences arising from the different definitions of mixed layer. Figure 9 suggests that

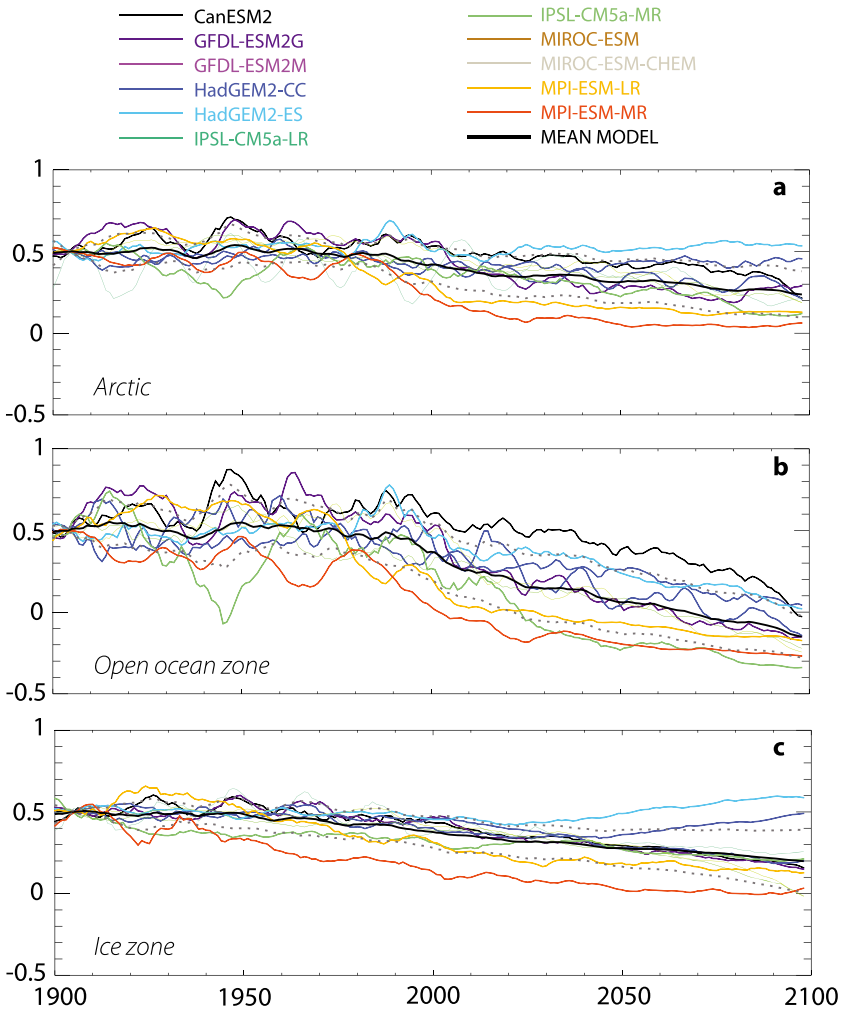

Figure 9. Time series of the stratification index (a normalized measure of the seasonal maximum mixed layer depth, see text for definition) for (a) the entire domain, (b) the open ocean zone, and (c) the ice zone; for all models and the mean model.

mixed layer depth decreases over the whole Arctic, and in both, the open ocean and sea ice zones over the 21st century. Notable exceptions are the HadGEM models which have increasing mixed layer depths from ~ 2030 onward in the sea ice zone. Regionally, mixing is not always decreasing everywhere: it increases in several coastal and shelf areas (not shown), but the regional average is dominated by the mixed layer shallowing in the central basin.

[49] Increasing stratification contributes to reduce the pre-bloom nutrient stocks. A simple correlation analysis (Table 4) indicates that the variance in annual mean Arctic $h_{mld}^{\max}$ explains more than 60% of the variance in NO_3 variance for seven models over 11. The two largest exceptions are the HadGEM models, which also feature some of the smallest mixed layer depth standard deviations. For the IPSL models, mixed layer variations explain only about 50% of the NO_3 changes, but the latter are the smallest in the model sample.

[50] In neighboring regions of the North Atlantic and Pacific Oceans (>50°N), surface NO_3 also decreases. The mean model rate of decrease of about 2 mmol/m^3/century for both regions is very similar to the 2.3 mmol/m^3/century in the Arctic Region. Correlations between the surface Arctic

Table 4. Correlation Statistics of Annual Mean Surface NO_3 and Seasonal Maximum Mixed Layer Depth $h_{mld}^{\max}$ (Averaged Over the Whole Domain)[a]

Model	σ_{NO_3} (mmol/m^3)	$\sigma_{h_{mld}^{\max}}$ (m)	r_{XY}	r_{XY}^2
CanESM2	1.4	12.5	0.8	0.6
GFDL-ESM2G	1.1	17.4	0.9	0.8
GFDL-ESM2M	0.8	13.1	0.9	0.8
HadGEM2-CC	1.0	5.4	0.5	0.3
HadGEM2-ES	0.8	5.6	–0.3	0.1
IPSL-CM5A-LR	0.4	14.6	0.7	0.5
IPSL-CM5A-MR	0.5	14.7	0.7	0.5
MIROC-ESM	1.1	11.9	0.9	0.9
MIROC-ESM-CHEM	1.1	13.6	0.9	0.9
MPI-ESM-LR	1.7	38.6	0.8	0.7
MPI-ESM-MR	1.8	42.3	0.8	0.6
Mean Model	1.0	12.8	1.0	0.9

[a]Computed from annual mean time series over 1900–2100: standard deviations (σ_{NO_3}, $\sigma_{h_{mld}^{\max}}$), raw and squared Pearson correlation coefficient r_{XY}.

NO_3 and corresponding values for the North Atlantic (mean c.c. = 0.89) and the North Pacific (0.87) are >0.8 for every model. This suggests a substantial contribution of the Pacific and Atlantic waters flowing to the Arctic NO_3 trend. Changes in the intensity of the ocean circulation could also affect nutrient supply to the Arctic, as the consistent decrease in the Atlantic Meridional Overturning Circulation intensity found throughout the 21st century in 10 CMIP5 models [*Cheng et al.*, 2013].

4. Discussion and Conclusions

[51] The response of primary production to future climate change in the Arctic Ocean analyzed here is inconsistently simulated by 11 ESMs used in the framework of the CMIP5 exercise. Among these models, three models predict a steady increase in Arctic-integrated primary production, and eight models have an initial increase followed by a decrease in the course of the 21st century. For three models among those eight, the decrease is sufficient to reach, by 2080–2099, integrated primary production levels that are below those simulated for 1980–1999. This result was envisioned by *Popova et al.* [2012], using five ice-ocean models (none is fully part of the CMIP5 models used here) forced by atmospheric reanalyses and ran over the recent past in the framework of the Arctic Ocean Model Intercomparison Project (AOMIP). This result was also apparent in the previous generation CMIP3 models [*Steinacher et al.*, 2010]. In any case, the potential for Arctic primary production increase (mean model +58 TgC/yr) appears to be for most models much smaller than the $\sim$ 300 TgC/yr obtained from a simple linear extrapolation of observed trends [*Arrigo and van Dijken*, 2011], because limitation by nitrate stocks is playing a primary role.

[52] Indeed, uncertainties in Arctic future primary production change for the 21st century are primarily driven by the large range in initial NO_3 levels. Whereas NO_3 consistently decreases over 1900–2100, models reach oligotrophy very early in the 20th century, or not even before 2100, because of this initial NO_3 scatter. This scatter directly stems from differences in the equilibrium state of ocean biogeochemical model components, reached after several thousand years of "spin-up" simulations, and used to initialize the CMIP5 simulations. In contrast, the scatter in the time of disappearance of perennial ice does is minor (2021–2076) and does not seem to affect uncertainties. However, the sea ice zone is the largest contributor to Arctic primary production and is where uncertainties in the sign of primary production changes are most visible. In the open ocean zones, virtually, all models agree on which changes to expect in the 21st century: more integrated PP due to wider open ocean zone, replacing less-productive portions of the ice zone; and less PP per unit area due to less nitrate.

[53] Despite the large uncertainties, the same mechanisms are at play in all models. Models agree on less perennial sea ice (hence, more light) and less nitrate in the course of the 21st century. Why nitrate decreases was not identified. But an associated increase in stratification, and simultaneous nitrate reductions in the North Atlantic and the North Pacific Oceans were identified as potential contributors. Either way, the simulated future physical ocean regime—through mixing, upwelling or eddy supplies—is overall not able to promote recurrent nitrate renewal, compensating for the losses due to increased primary production and export to depth.

[54] The agreement on the general mechanisms at play gives hope, since reducing the uncertainty on the present observed and simulated nutrient status in the Arctic Ocean, would render projections much more consistent. Nitrate data are scarce in the Arctic, but a few profiles exist and their recent analysis broadly indicates what are the spatial and seasonal patterns in the Arctic [*Codispoti et al.*, 2013]. Future model calibrations should at least use these observations as a baseline evaluation. Collecting an exhaustive Arctic observational NO_3 climatology is already beyond reach because of recent changes. However, assessing the levels of pre-bloom present Arctic nitrate stocks is important, and it might still be possible to collect pre-bloom NO_3 observations, which do not deviate too far from the 20th century climatology. In this context, a minimal requirement for data collection would be to get pre- and post-bloom NO_3 profiles at a few well-chosen locations (or over an Arctic transect) and over a few years. Optical nitrate sensors are promising tools to accomplish this goal [see, e.g., *McLaughlin and Carmack*, 2010].

[55] In addition, an evaluation and an improvement of the model mechanisms influencing NO_3 and more generally PP in the Arctic are required. The model equilibrium state expresses a combined response to ocean circulation and biogeochemical parameterizations and their tuning. Hence, three natural directions of model improvement seem suitable: (i) a better model representation of ocean circulation and ice distribution; (ii) a better representation of Arctic biogeochemical processes, in particular in the sea ice zone; and (iii) improved calibration of the equilibrium state of the ocean biogeochemical model components. The Arctic Ocean circulation far from being fully covered by observations, and its simulation is challenging. Large intermodel differences in stratification, stratification type, and ocean circulation—which are the main physical NO_3 drivers—were found among nine AOMIP models [*Holloway et al*., 2007].

[56] The large uncertainties in the sea ice zone suggest that the part of the problem could be linked to sea ice. Some of the expectedly major physical effects of sea ice on ocean biogeochemistry—namely, the input of brine and freshwater due to sea ice growth and melt, and the barrier role of sea ice to wind stirring of the water column—have at least a first-order model representation. However, several sea ice processes relevant to ocean biogeochemistry are neither properly understood nor represented in ESMs [*Vancoppenolle et al.*, 2013]. First, sea ice is a host for microbial communities [*Thomas and Dieckmann*, 2010], and stores nutrients, organic material, and iron [e.g., *Lancelot et al.*, 2009; *Vancoppenolle et al.*, 2010], which are released during sea ice melt. To address that issue, some groups are developing biogeochemical sea ice components for large-scale Earth system studies [e.g., *Deal et al.*, 2011]. Second, the model representation of light transmission through sea ice has generally not been developed for biogeochemistry problems, leading to significant uncertainties in under-ice light fields [see, e.g., *Lavoie et al.*, 2005]. Under-ice light fields are likely a primary factor in the trigerring of under-ice blooms, which importance has recently been re-evaluated

[*Mundy et al*., 2009; *Arrigo et al*., 2012]. Other Arctic biogeochemical processes in the sea ice zone deserving more consideration from modelers include land-ocean interactions, in particular the large and fast changing riverine inputs [*Peterson et al.*, 2006] spreading on the wide Arctic continental shelves [e.g., *McClelland et al.*, 2007]. Rivers are likely not the primary actor, though, since the riverine contribution of nitrate to new production is very small at regional scales and negligible at the pan-Arctic scale [*Le Fouest et al.*, 2012]. The representation of benthic nutrient cycling is also generally absent from models, which could matter on the wide Arctic shallow shelves.

[57] The evolution of primary production in the Arctic Ocean may have consequences on important ecosystem services, such as marine resources (i.e., fisheries) and the ocean anthropogenic carbon sink. Estimates of total marine (and estuarine) fish catches in the Arctic Ocean (FAO Area 18) amounts to 10,200 t/yr by the mid-2000s [*Zeller et al.*, 2011]. This is very low when compared to other Large Marine Ecosystem areas of the world ocean, but these resources are an important part of food security in that region and have essential cultural significance. Current expectations are that increased accessibility of Arctic areas, as well as enhanced primary production due to reduced sea-ice cover, could result in increased fish catches in the coming decades [*Tremblay et al.*, 2012]. Our analysis shows that climate change impacts on PP in the Arctic Ocean are quite uncertain and that increased oligotrophy could limit a potential light-driven increase in PP, and hence the existence of any large-scale commercial fisheries. In addition, recent observations suggest that the expected physical (stratification) and chemical (oligotrophy) changes could benefit small picophytoplankton cells at the expense of large diatoms [*Li et al.*, 2009] which would support lower export of biogenic carbon for extraction (e.g., harvest).

[58] According to the compilation of *Bates and Mathis* [2009], the Arctic Ocean presently takes up from 66 to 199 TgC/yr from the atmosphere, thus contributing to the ocean anthropogenic carbon uptake. The Arctic Ocean CO_2 sink has likely been increasing due to sea ice retreat: from 24 to 66 TgC/yr over 1972–2002 according to observational estimates [*Bates et al.*, 2006], and by $\sim$10 TgC/yr over 1997–2007 following a model study [*McGuire et al.*, 2010]. How the Arctic Ocean CO_2 sink will evolve in the future is not presently clear. On the one hand, potential increase in PP in the Arctic Ocean due to sea ice retreat could drive increases in new production or net community production, and hence a DIC drawdown that should increase the air-sea CO_2 disequilibrium (i.e., ΔCO_2) and increase the net oceanic uptake of CO_2 [*Bates and Mathis*, 2009]. On the other hand, shallow mixed layers, reduced sea ice cover, strong stratification, and relatively small biological production in low nutrient conditions can result in a quick increase of CO_2 in Arctic waters, decreasing the air-sea CO_2 difference which may limit the future efficiency of the Arctic CO_2 sink. Such a setting has been observed in 2008 in the Canadian Basin by *Cai et al.* [2010]. In the end, the future of the Arctic CO_2 sink will be determined by the modified seasonality of its driving factors [see, e.g., *Steiner et al.*, 2013], in a complex combination that cannot be easily predicted [*Bates and Mathis*, 2009]. The inconsistency of the future projections of PP and oligotrophy in the Arctic Ocean shown in this paper casts further doubt upon the sign of the impact of changes in the biological pump on anthropogenic carbon uptake in the coming decades.

[59] **Acknowledgments.** Valuable help from François Massonnet, Pierre-Yves Barriat, Camille Lique, Roland Séférian, Ivan Grozny, Ioulia Nikolskaia, Hideki Okajima, and Michio Kawamiya; and financial support from project BISICLO FP7 CIG 321938 are gratefully acknowledged. We also acknowledge the World Climate Research Programme's Working Group on Coupled Modelling, which is responsible for CMIP5, and we thank the climate modeling groups for producing and making their model output available. For CMIP5, the U.S. Department of Energy's Program for Climate Model Diagnosis and Intercomparison provides coordinating support and led development of software infrastructure in partnership with the Global Organization for Earth System Science Portals. Here the French Portal Prodiguer from the Institut Pierre-Simon Laplace, Paris, France, was used to download CMIP5 output with great efficiency. Three groups are warmly thanked for providing data and associated support: EUMETSAT-OSISAF (sea ice concentration), the National Oceanographic Data Center (World Ocean Atlas nitrate), as well as Kevin Arrigo and Gert van Dijken (Arctic primary production), The two anonymous reviewers and the editor are warmly thanked for their significant contribution to this manuscript.

References

Alexander, V., and H. J. Niebauer (1981), Oceanography of the easter Bering Sea ice-edge zone in spring, *Limnol. Oceanogr.*, *26*(6), 1111–1125.

Arora, V. K., J. F. Scinocca, G. J. Boer, J. R. Christian, K. L. Denman, G. M. Flato, V. V. Kharin, W. G. Lee, and W. J. Merryfield (2011), Carbon emission limits required to satisfy future representative concentration pathways of greenhouse gases, *Geophys. Res. Lett.*, *38*, L05805, doi:10.1029/2010GL046270.

Arrigo, K. R., and G. van Dijken (2011), Secular trends in Arctic Ocean net primary production, *J. Geophys. Res.*, *116*, C09011, doi:10.1029/2011JC007151.

Arrigo, K. R., et al. (2012), Massive phytoplankton blooms under Arctic sea ice, *Science*, *336*, 1408–1409.

Aumont, O., E. Maier-Reimer, S. Blain, and P. Monfray (2003), An ecosystem model of the global ocean including Fe, Si, P colimitations, *Global Biogeochem. Cycles*, *17*(2), 1060, doi:10.1029/2001GB001745.

Bates, N. R., and J. T. Mathis (2009), The Arctic Ocean marine carbon cycle: Evaluation of air-sea CO_2 exchanges, ocean acidification impacts and potential feedbacks, *Biogeosciences*, *6*(11), 2433–2459, doi:10.5194/bg-6-2433-2009.

Bates, N. R., S. B. Moran, D. A. Hansell, and J. T. Mathis (2006), An increasing CO_2 sink in the Arctic Ocean due to sea-ice loss, *Geophys. Res. Lett.*, *33*, L23609, doi:10.1029/2006GL027028.

Cai, W.-J., et al. (2010), Decrease in the CO_2 uptake capacity in an ice-free Arctic Ocean basin, *Science*, *329*(5991), 556–559, doi:10.1126/science.1189338.

Carmack, E., and F. McLaughlin (2011), Towards recognition of physical and geochemical change in subarctic and Arctic seas, *Prog. Oceanogr.*, *90*, 90–104, doi:10.1016/j.pocean.2011.02.007.

Carmack, E., and P. Wassmann (2006), Food webs and physical, biological coupling on pan-Arctic shelves: Unifying concepts and comprehensive perspectives, *Prog. Oceanogr.*, *71*(2–4), 446–477, doi:10.1016/j.pocean.2006.10.004.

Cheng, W., J. C. Chiang, and D. Zhang (2013), Atlantic meridional overturning circulation (AMOC) in CMIP5 models: RCP and historical simulations, *J. Clim.*, doi:10.1175/JCLI-D-12-00496.1.

Christian, J. R., et al. (2010), The global carbon cycle in the Canadian Earth system model (CanESM1) preindustrial control simulation, *J. Geophys. Res.*, *115*, G03014, doi:10.1029/2008JG000920.

Codispoti, L., V. Kelly, A. Thessen, P. Matrai, S. Suttles, V. Hill, M. Steele, and B. Light (2013), Synthesis of primary production in the Arctic Ocean: III. Nitrate and phosphate based estimates of net community production, *Prog. Oceanogr.*, *110*(0), 126–150, doi:10.1016/j.pocean.2012.11.006.

Collins, W. J., et al. (2011), Development and evaluation of an Earth-System model-HadGEM2, *Geosci. Model Dev.*, *4*(4), 1051–1075, doi:10.5194/gmd-4-1051-2011.

Deal, C., M. Jin, S. Elliott, E. Hunke, M. Maltrud, and N. Jeffery (2011), Large-scale modeling of primary production and ice algal biomass within Arctic sea ice in 1992, *J. Geophys. Res.*, *116*, C07004, doi:10.1029/2010JC006409.

Dufresne, J.-L., et al. (2013), Climate change projections using the IPSL-CM5 Earth System Model: From CMIP3 to CMIP5, *Clim. Dyn.*, *40*, 2123–2165, doi:10.1007/s00382-012-1636-1.

Dunne, J. P., et al. (2012), GFDL's ESM2 global coupled climate-carbon Earth System Models Part I: Physical formulation and baseline simulation characteristics, *J. Clim.*, *25*, 6646–6665.

Dunne, J. P., et al. (2013), GFDL's ESM2 global coupled climate-carbon Earth System Models Part II: Carbon system formulation and baseline simulation characteristics, *J. Clim.*, *26*(7), 2247–2267, doi:10.1175/JCLI-D-12-00150.1.

Garcia, H. E., R. A. Locarnini, T. P. Boyer, J. I. Antonov, M. M. Zweng, O. K. Baranova, and D. R. Johnson (2010), *World Ocean Atlas 2009,* vol. 4, *Nutrients (Phosphate, Nitrate, Silicate),* U.S. Gov. Print. Off., Washington, D. C.

HadGEM2 Team (2011), The HadGEM2 family of Met Office Unified Model climate configurations, *Geosci. Model Dev.*, *4*(3), 723–757, doi:10.5194/gmd-4-723-2011.

Hill, V. J., P. A. Matrai, E. Olson, S. Suttles, M. Steele, L. Codispoti, and R. C. Zimmerman (2013), Synthesis of integrated primary production in the Arctic Ocean: II. In situ and remotely sensed estimates, *Prog. Oceanogr., 110*, 107–125, doi:10.1016/j.pocean.2012.11.005.

Holland, M. M., C. M. Bitz, E. C. Hunke, W. H. Lipscomb, and J. Schramm (2006), Influence of the sea ice thickness distribution on polar climate in CCSM3, *J. Clim.*, *19*, 2398–2414.

Holloway, G., et al. (2007), Water properties and circulation in Arctic Ocean models, *J. Geophys. Res.*, *112*, C04S03, doi:10.1029/2006JC003642.

Ilyina, T., K. D. Six, J. Segschneider, E. Maier-Reimer, H. Li, and I. Nunez-Riboni (2013), The global ocean biogeochemistry model HAMOCC: Model architecture and performance as component of the MPI-Earth System Model in different CMIP5 experimental realizations, *J. Adv. Model. Earth Syst.*, *5*, 287–315, doi:10.1029/2012MS000178.

Kahru, M., V. Brotas, M. Manzano-Sarabia, and B. G. Mitchell (2011), Are phytoplankton blooms occurring earlier in the Arctic?, *Global Change Biol.*, *17*, 1733–1739, doi:10.1111/j.1365-2486.2010.02312.x.

Kawamiya, M., M. J. Kishi, and N. Suginohara (2000), An ecosystem model for the North Pacific embedded in a general circulation model Part I: Model description and characteristics of spatial distributions of biological variables, *J. Mar. Syst.*, *25*, 129–157.

Kwok, R., and D. Rothrock (2009), Decline in Arctic sea ice thickness from submarine and ICESat records: 1958–2008, *Geophys. Res. Lett.*, *36*, L15501, doi:10.1029/2009GL039035.

Lancelot, C., A. de Montety, H. Goosse, S. Becquevort, V. Schoemann, B. Pasquer, and M. Vancoppenolle (2009), Spatial distribution of the iron supply to phytoplankton in the Southern Ocean: A model study, *Biogeosciences*, *6*, 2861–2878.

Lavoie, D., K. Denman, and C. Michel (2005), Modeling ice algal growth and decline in a seasonally ice-covered region of the Arctic (Resolute Passage, Canadian Archipelago), *J. Geophys. Res.*, *110*, C11009, doi:10.1029/2005JC002922.

Le Fouest, V., M. Babin, and J.-E. Tremblay (2012), The fate of riverine nutrients on Arctic shelves, *Biogeosci. Discuss.*, *9*, 13,397–13,437.

Li, W. K., F. A. McLaughlin, C. Lovejoy, and E. C. Carmack (2009), Smallest algae thrive as the Arctic Ocean freshens, *Science*, *326*, 539.

Maslanik, J. A., C. Fowler, J. Stroeve, S. Drobot, J. Zwally, and W. Emery (2007), A younger, thinner arctic ice cover: Increased potential for rapid, extensive sea-ice loss, *Geophys. Res. Lett.*, *34*, L24501, doi:10.1029/2007GL032043.

Massonnet, F., T. Fichefet, H. Goosse, M. Vancoppenolle, P. Mathiot, and C. König-Beatty (2011), On the influence of model physics on simulations of Arctic and Antarctic sea ice, *Cryosphere*, *5*, 687–699, doi:10.5194/tc-5-687-2011.

Massonnet, F., T. Fichefet, H. Goosse, C. M. Bitz, G. Philippon-Berthier, M. M. Holland, and P.-Y. Barriat (2012), Constraining projections of summer Arctic sea ice, *Cryosphere*, *6*, 1383–1394.

McClelland, J. W., M. Stieglitz, F. Pan, R. M. Holmes, and B. J. Peterson (2007), Recent changes in nitrate and dissolved organic carbon export from the Upper Kuparuk River, North Slope, Alaska, *J. Geophys. Res.*, *112*, G04S60, doi:10.1029/2006JG000371.

McGuire, A. D., et al. (2010), An analysis of the carbon balance of the Arctic basin from 1997 to 2006, *Tellus, Ser. B*, *62*(5), 455–474, doi:10.1111/j.1600-0889.2010.00497.x.

McLaughlin, F. A., and E. C. Carmack (2010), Deepening of the nutricline and chlorophyll maximum in the Canada basin interior, 2003–2009, *Geophys. Res. Lett.*, *37*, L24602, doi:10.1029/2010GL045459.

Moss, R. H., et al. (2010), The next generation of scenarios for climate change research and assessment, *Nature*, *463*, 747–756.

Mundy, C. J., M. Gosselin, C. Nozais, and M. Simard (2009), Characterization of bottom ice algal and detrital spectral absorption properties in first-year sea ice of an Arctic polynya, in *Eos Trans. AGU,* 90(52), Fall Meet. Suppl., Abstract C41C-0469.

Pabi, S., G. L. van Dijken, and K. R. Arrigo (2008), Primary production in the Arctic Ocean, 1998–2006, *J. Geophys. Res.*, *113*, C08005, doi:10.1029/2007JC004578.

Peterson, B. J., J. McClelland, R. Curry, R. M. Holmes, J. E. Walsh, and K. Aagaard (2006), Trajectory shifts in the Arctic and Subarctic freshwater cycle, *Science*, *313*, 1061–1066.

Popova, E. E., A. Yool, A. C. Coward, F. Dupont, C. Deal, S. Elliott, E. Hunke, M. Jin, M. Steele, and J. Zhang (2012), What controls primary production in the Arctic Ocean? Results from an intercomparison of five general circulation models with biogeochemistry, *J. Geophys. Res.*, *117*, C00D12, doi:10.1029/2011JC007112.

Popova, E. E., A. Yool, Y. Aksenov, and A. C. Coward (2013), Role of advection in Arctic Ocean lower trophic dynamics: A modeling perspective, *J. Geophys. Res. Oceans*, *118*, 1571–1586, doi:10.1002/jgrc.20126.

Sarthou, G., K. R. Timmermans, S. Blain, and P. Tréguer (2005), Growth physiology and fate of diatoms in the ocean: A review, *J. Sea Res.*, *53*, 25–42.

Semtner, A. J. (1976), A model for the thermodynamic growth of sea ice in numerical investigations of climate, *J. Phys. Oceanogr.*, *6*, 379–389.

Stammerjohn, S., R. Massom, D. Rind, and D. Martinson (2012), Regions of rapid sea ice change: An inter-hemispheric seasonal comparison, *Geophys. Res. Lett.*, *39*, L06501, doi:10.1029/2012GL050874.

Steinacher, M., et al. (2010), Projected 21st century decrease in marine productivity: A multi-model analysis, *Biogeosciences*, *7*, 979–1005.

Steiner, N. S., W. G. Lee, and J. R. Christian (2013), Enhanced gas fluxes in small sea ice leads and cracks–Effects on CO_2 exchange and ocean acidification, *J. Geophys. Res. Oceans*, *118*, 1195–1205, doi:10.1002/jgrc.20100.

Stroeve, J. C., V. Kattsov, A. Barrett, M. Serreze, T. Pavlova, M. Holland, and W. N. Meier (2012), Trends in Arctic sea ice extent from CMIP5, CMIP3 and observations, *Geophys. Res. Lett.*, *39*, L16502, doi:10.1029/2012GL052676.

Taylor, K. E., R. J. Stouffer, and G. A. Meehl (2012), An overview of CMIP5 and the experiment design, *Bull. Am. Meteorol. Soc.*, *93*(4), 485–498, doi:10.1175/BAMS-D-11-00094.1.

Thomas, D. N., and G. Dieckmann (eds.) (2010), *Sea Ice*, 2nd ed., 619 pp., Wiley-Blackwell, Oxford, UK.

Tonboe, R., S. Eastwood, T. Lavergne, and L. T. Pedersen (2011), EUMETSAT OSI SAF global sea ice concentration reprocessing data, Natl. Snow and Ice Data Cent., Boulder, Colo.

Tremblay, J.-E., and J. Gagnon (2009), The effect of irradiance and nutrient supply on the productivity of Arctic waters: A perspective on climate change, in *Influence of Climate Change on the Changing Arctic and Sub-Arctic Conditions*, edited by J. C. J. Nihoul and A. G. Kostianoy, pp. 73–94, Springer, New York.

Tremblay, J.-E., K. Simpson, J. Martin, L. Miller, Y. Gratton, D. Barber, and N. M. Price (2008), Vertical stability and the annual dynamics of nutrients and chlorophyll fluorescence in the coastal, southeast Beaufort Sea, *J. Geophys. Res.*, *113*, C07S90, doi:10.1029/2007JC004547.

Tremblay, J.-E., D. Robert, D. E. Varela, C. Lovejoy, G. Darnis, R. J. Nelson, and A. R. Sastri (2012), Current state and trends in Canadian Arctic marine ecosystems: I. Primary production, *Clim. Change*, *115*, 161–178, doi:10.1007/s10584-012-0496-3.

University of Colorado at Boulder, B. (2012), Arctic sea ice reaches lowest extent ever recorded, *Science Daily*, 27 Aug. [Available at http://www.sciencedaily.com/releases/2012/08/120827130726.htm].

Vancoppenolle, M., H. Goosse, A. de Montety, T. Fichefet, B. Tremblay, and J.-L. Tison (2010), Modeling brine and nutrient dynamics in Antarctic sea ice: The case of dissolved silica, *J. Geophys. Res.*, *115*, C02005, doi:10.1029/2009JC005369.

Vancoppenolle, M., et al. (2013), Role of sea ice in global biogeochemical cycles: Emerging views and challenges, *Quat. Sci. Rev.*, doi:10.1016/j.quascirev.2013.04.011, in press.

Wassmann, P., and M. Reigstad (2011), Future Arctic Ocean seasonal ice zones and implications for pelagic-benthic coupling, *Oceanography*, *24*(3), 220–231, doi:10.5670/oceanog.2011.74.

Watanabe, S., et al. (2011), MIROC-ESM 2010: Model description and basic results of CMIP5-20c3m experiments, *Geosci. Model Dev.*, *4*(4), 845–872, doi:10.5194/gmd-4-845-2011.

Winton, M. (2000), A reformulated three-layer sea ice model, *J. Atmos. Oceanic Technol.*, *17*, 525–531.

Zeller, D., S. Booth, E. Pakhomov, W. Swartz, and D. Pauly (2011), Arctic fisheries catches in Russia, USA, and Canada: Baselines for neglected ecosystems, *Polar Biol.*, *34*, 955–973, doi:10.1007/s00300-010-0952-3.